J|A|C|S ARTICLES

Published on Web 12/02/2010

Fundamentals of Melt Infiltration for the Preparation of Supported Metal Catalysts. The Case of Co/SiO_2 for Fischer−Tropsch Synthesis

Tamara M. Eggenhuisen, Johan P. den Breejen, Dirkjan Verdoes, Petra E. de Jongh, and Krijn P. de Jong*

Inorganic Chemistry and Catalysis, Debye Institute for Nanomaterials Science, Utrecht University, Sorbonnelaan 16, 3584 CA Utrecht, The Netherlands

Received September 7, 2010; E-mail: k.p.dejong@uu.nl

Abstract: We explored melt infiltration of mesoporous silica supports to prepare supported metal catalysts with high loadings and controllable particle sizes. Melting of $Co(NO_3)_2 \cdot 6H_2O$ in the presence of silica supports was studied in situ with differential scanning calorimetry. The melting point depression of the intraporous phase was used to quantify the degree of pore loading after infiltration. Maximum pore-fillings corresponded to 70−80% of filled pore volume, if the intraporous phase was considered to be crystalline $Co(NO_3)_2 \cdot 6H_2O$. However, diffraction was absent in XRD both from the ordered mesopores at low scattering angles and from crystalline cobalt nitrate phases at high angles. Hence, an amorphous, lower density, intraporous $Co(NO_3)_2 \cdot 6H_2O$ phase was proposed to fill the pores completely. Equilibration at 60 °C in a closed vessel was essential for successful melt infiltration. In an open crucible, dehydration of the precursor prior to infiltration inhibited homogeneous filling of support particles. The dispersion and distribution of Co_3O_4 after calcination could be controlled using the same toolbox as for preparation via solution impregnation: confinement and the calcination gas atmosphere. Using ordered mesoporous silica supports as well as an industrial silica gel support, catalysts with Co metal loadings in the range of 10−22 wt % were prepared. The Co_3O_4 crystallite sizes ranged from 4 to 10 nm and scaled with the support pore diameters. By calcination in N_2, pluglike nanoparticles were obtained that formed aggregates over several pore widths, while calcination in 1% NO/N_2 led to the formation of smaller individual nanoparticles. After reduction, the Co/SiO_2 catalysts showed high activity for the Fischer−Tropsch synthesis, illustrating the applicability of melt infiltration for supported catalyst preparation.

Introduction

In the past, supported catalyst preparation has been referred to as an art rather than science. However, nowadays the limits and possibilities of the classical preparation routes are being studied at a fundamental level.[1,2] The literature on impregnation and drying,[3−5] deposition−precipitation,[6−8] and ion-adsorption[9−11] is extensive. Nevertheless, control over metal nanoparticle size, distribution, and even shape in order to maximize catalytic effectiveness persists as a motivation for designing new or improved preparation routes.[12,13] Many alternative methods, such as chemical vapor deposition,[14] atomic layer deposition,[15] surface functionalization,[16,17] or combined approaches have been developed. Still, impregnation and drying with metal nitrate salts as a precursor is the most widely applied preparation method. It is favored because of its convenience and the use of highly soluble, low cost precursors that readily decompose. Unfortunately, often catalysts are obtained with an inhomogeneous metal dispersion and distribution, due to low support−precursor interactions.[18−21]

(1) *Catalyst Preparation−Science and Engineering*; Regalbuto, J. R., Ed.; CRC Press: Boca Raton, 2007.
(2) *Synthesis of Solid Catalysts*; De Jong, K. P., Ed.; Wiley-VCH: Weinheim, 2009.
(3) van Dillen, A. J.; Terorde, R. J. A. M.; Lensveld, D. J.; Geus, J. W.; de Jong, K. P. *J. Catal.* **2003**, *216*, 257–264.
(4) Lekhal, A.; Glasser, B. J.; Khinast, J. G. *Chem. Eng. Sci.* **2004**, *59*, 1063–1077.
(5) Bergwerff, J. A.; Visser, T.; Leliveld, B. R. G.; Rossenaar, B. D.; de Jong, K. P.; Weckhuysen, B. M. *J. Am. Chem. Soc.* **2004**, *126*, 14548–14556.
(6) Che, M.; Cheng, Z. X.; Louis, C. *J. Am. Chem. Soc.* **1995**, *117*, 2008–2018.
(7) Burattin, P.; Che, M.; Louis, C. *J. Phys. Chem. B* **1999**, *103*, 6171–6178.
(8) van der Lee, M. K.; van Dillen, A. J.; Bitter, J. H.; de Jong, K. P. *J. Am. Chem. Soc.* **2005**, *127*, 13573–13582.
(9) Hartmann, M.; Poppl, A.; Kevan, L. *J. Phys. Chem.* **1996**, *100*, 9906–9910.
(10) Schreier, M.; Regalbuto, J. R. *J. Catal.* **2004**, *225*, 190–202.
(11) Jiao, L.; Regalbuto, J. R. *J. Catal.* **2008**, *260*, 329–341.
(12) Bell, A. T. *Science* **2003**, *299*, 1688–1691.
(13) Somorjai, G. A.; Tao, F.; Park, J. Y. *Top. Catal.* **2008**, *47*, 1–14.
(14) Serp, P.; Kalck, P.; Feurer, R. *Chem. Rev.* **2002**, *102*, 3085–3128.
(15) Lu, J. L.; Stair, P. C. *Angew. Chem., Int. Ed.* **2010**, *49*, 2547–2551.
(16) Tu, C. H.; Wang, A. Q.; Zheng, M. Y.; Wang, X. D.; Zhang, T. *Appl. Catal. A-Gen.* **2006**, *297*, 40–47.
(17) Cutrufello, M. G.; Rombi, E.; Cannas, C.; Casu, M.; Virga, A.; Fiorilli, S.; Onida, B.; Ferino, I. *J. Mater. Sci.* **2009**, *44*, 6644–6653.
(18) Mile, B.; Stirling, D.; Zammitt, M. A.; Lovell, A.; Webb, M. *J. Catal.* **1988**, *114*, 217–229.
(19) Panpranot, J.; Goodwin, J. G.; Sayari, A. *Catal. Today* **2002**, *77*, 269–284.
(20) Girardon, J. S.; Lermontov, A. S.; Gengembre, L.; Chernavskii, P. A.; Griboval-Constant, A.; Khodakov, A. Y. *J. Catal.* **2005**, *230*, 339–352.

10.1021/ja1080508

Melt infiltration can be considered as an alternative to impregnation and drying. Metal salts that melt before they decompose can be introduced to a porous support via capillary forces without the use of a solvent. Hydrated transition metal nitrates are particularly suitable, since they have low melting points coined to dissolution in crystal water.[22] Melt infiltration appears in literature under various names, such as the solvent-free method,[23,24] solid-state grinding[25] or the solid−liquid route.[22,26] In the field of catalyst preparation, it has been applied to obtain highly dispersed copper species on SBA-15[23,27] as well as on ZSM-5.[28] However, melt infiltration of MCM-41 with iron nitrate resulted in large extraporous crystallites.[29] Melt infiltration with cobalt nitrate salt has been used with extrudates to obtain an egg-shell catalyst, where the high viscosity of the nitrate melt was used to obtain an inhomogeneous precursor distribution.[30] In the field of nanocasting,[31] this procedure was used to obtain mesoporous silica with a high loading and after calcination a highly agglomerated metal oxide to form mesoporous single crystals.[25,26,32] Melt infiltration with metals is applied in materials science for the preparation of ceramic composites or hydrogen storage materials.[33−35]

Although melt infiltration has been applied to prepare supported metal oxides, the fundamental phenomena have remained obscure and erratic results were sometimes obtained. Insights relied on information obtained after calcination or the disappearance of the precursor diffraction pattern after heat treatment. In addition, the potential of melt infiltration to tune the dispersion and distribution of the metal oxide for catalytic applications has not been studied.

Differential scanning calorimetry (DSC) gives direct information on the melting behavior of the precursor salt and its interaction with a porous support. Salt confined in a mesoporous system can be distinguished from extraporous phases due to the depressed melting point.[36] This technique has been applied to study water or aqueous solutions confined in mesoporous silica,[37,38] and the melting point depression of confined salt hydrates was also studied with ^{1}H NMR.[39] In addition, the phases can be quantified through the specific melting enthalpy. This allows direct evaluation of precursor infiltration.

In this work, the applicability of melt infiltration to obtain highly loaded supported catalysts with controllable nanoparticle size is discussed. The extent of pore-filling was studied with DSC as well as effects of the melt infiltration conditions on the precursor loading. In addition, low- and high-angle XRD and TEM were used to determine the precursor distribution. The versatility of melt infiltration for supported catalyst preparation was illustrated by the preparation of a series of Co/SiO_2 catalysts for the Fischer−Tropsch synthesis with ordered mesoporous silica as model supports and a commercial silica gel as example of an industrial support. The same preparation toolbox was employed as for solution impregnation to control dispersion and distribution of the cobalt oxide particles, i.e., via confinement and calcination.[40]

Experimental Section

Support Preparation. SBA-15 was synthesized according to the procedure described by Zhao et al. using P123 as template and tetraethylorthosilicate (98%, Aldrich) as silica source.[41] A gel with molar ratio of 1 SiO_2:0.0143 P123:5.05 HCl:144 H_2O was aged under stirring at 40 °C for 20 h after which it was treated at 50, 100, or 120 °C in a Teflon-lined steel autoclave for 48 h under static conditions. After filtration and washing, the samples were dried at 120 °C and subsequently calcined at 550 °C (1 °C/min, 6 h). Samples prepared at different temperatures are denoted as S50, S100, and S120.

Large pore MCM-41 was synthesized using a procedure described by Cheng et al. with cetyltrimethylammoniumbromide (CTAB, Aldrich) as template, Aerosil 380 (Degussa) as silica source and tetramethyl ammonium hydroxide (TMAOH, 25% Aldrich) as base.[42] All reactants were mixed at room temperature for 30 min until a homogeneous gel was obtained with the molar ratio 1 SiO_2: 0.25 CTAB: 0.20 TMAOH: 40 H_2O. The gel was aged in a Teflon-lined steel autoclave at 80 °C for 24 h and subsequently crystallized at 150 °C for 24 h. The product was filtered, washed with water and acetone, dried at 120 °C, and subsequently calcined at 550 °C (1 °C/min, 8 h).

A commercial silica gel, Davicat 1404 (Grace-Davidson) was used as obtained.

Catalyst Preparation. To prepare a typical catalyst, 802 mg $Co(NO_3)_2\cdot 6H_2O$ (>99.0%, Aldrich) and 592 mg of the support (S100), corresponding to a theoretical Co loading of 22 wt % in the reduced catalyst, were physically mixed in a mortar with a pestle for several minutes under ambient conditions until the powder was homogeneously pink. Mixtures of $Co(NO_3)_2\cdot 6H_2O$ and support are denoted by the mass loading of $Co(NO_3)_2\cdot 6H_2O$ in $g/g_{support}$, e.g., $Co(NO_3)_2\cdot 6H_2O$/S100 with 1.4 g/g_{S100} loading. In the same manner other supports were mixed with $Co(NO_3)_2\cdot 6H_2O$ to obtain the following catalysts Co/MCM (1.2 g/g_{MCM}, 19.9 wt % Co), Co/S50 (0.58 g/g_{S50}, 10.5 wt % Co), Co/S120 (1.3 g/g_{S120}, 21.2 wt % Co), and Co/silica gel (1.1 g/g_{SiO2}, 17.6 wt % Co). The reported cobalt loadings coincided with the maximum precursor loading that was determined with DSC (vide infra). Melt infiltration was performed

(21) Marceau, E.; Che, M.; Cejka, J.; Zukal, A. *Chemcatchem* **2010**, *2*, 413–422.
(22) Yue, W.; Zhou, W. Z. *Chem. Mater.* **2007**, *19*, 2359–2363.
(23) Zhou, C. F.; Wang, Y. M.; Cao, Y.; Zhuang, T. T.; Huang, W.; Chun, Y. A.; Zhu, J. H. *J. Mater. Chem.* **2006**, *16*, 1520–1528.
(24) Shon, J. K.; Kong, S. S.; Kim, Y. S.; Lee, J. H.; Park, W. K.; Park, S. C.; Kim, J. M. *Micropor. Mesopor. Mater.* **2009**, *120*, 441–446.
(25) Wang, Y. M.; Wu, Z. Y.; Wang, H. J.; Zhu, J. H. *Adv. Funct. Mater.* **2006**, *16*, 2374–2386.
(26) Zheng, M. B.; Cao, J.; Liao, S. T.; Liu, J. S.; Chen, H. Q.; Zhao, Y.; Dai, W. J.; Ji, G. B.; Cao, J. M.; Tao, J. *J. Phys. Chem. C* **2009**, *113*, 3887–3894.
(27) Wang, Y. M.; Wu, Z. Y.; Zhu, J. H. *J. Solid State Chem.* **2004**, *177*, 3815–3823.
(28) Xiao, F. S.; Zheng, S.; Sun, J. M.; Yu, R. B.; Qiu, S. L.; Xu, R. R. *J. Catal.* **1998**, *176*, 474–487.
(29) Schuth, F.; Wingen, A.; Sauer, J. *Micropor. Mesopor. Mater.* **2001**, *44*, 465–476.
(30) Iglesia, E.; Soled, S. L.; Baumgartner, J. E.; Reyes, S. C. *J. Catal.* **1995**, *153*, 108–122.
(31) Schuth, F. *Angew. Chem., Int. Ed.* **2003**, *42*, 3604–3622.
(32) Yue, W. B.; Hill, A. H.; Harrison, A.; Zhou, W. Z. *Chem. Commun.* **2007**, 2518–2520.
(33) Lai, S. W.; Chung, D. D. L. *J. Mater. Sci.* **1994**, *29*, 3128–3150.
(34) Liu, J. W.; Zheng, Z. X.; Wang, J. M.; Wu, Y. C.; Tang, W. M.; Lu, J. *J. Alloys Compd.* **2008**, *465*, 239–243.
(35) de Jongh, P. E.; Wagemans, R. W. P.; Eggenhuisen, T. M.; Dauvillier, B. S.; Radstake, P. B.; Meeldijk, J. D.; Geus, J. W.; de Jong, K. P. *Chem. Mater.* **2007**, *19*, 6052–6057.
(36) Brun, M.; Lallemand, A.; Quinson, J.-F.; Eyraud, C. *Thermochim. Acta* **1977**, *21*, 59–88.
(37) Schreiber, A.; Ketelsen, I.; Findenegg, G. H. *Phys. Chem. Chem. Phys.* **2001**, *3*, 1185–1195.
(38) Eggenhuisen, T. M.; van Steenbergen, M. J.; Talsma, H.; de Jongh, P. E.; de Jong, K. P. *J. Phys. Chem. C* **2009**, *113*, 16785–16791.
(39) Vargas-Florencia, D.; Petrov, O.; Furo, I. *J. Phys. Chem. B* **2006**, *110*, 3867–3870.
(40) Woltters, M.; van Grotel, L. J. W.; Eggenhuisen, T. M.; Sietsma, J. R. A.; de Jongh, P. E.; de Jong, K. P. *Catal. Today* 2010, doi: 10.1016/j.cattod.2010.02.052.
(41) Zhao, D. Y.; Huo, Q. S.; Feng, J. L.; Chmelka, B. F.; Stucky, G. D. *J. Am. Chem. Soc.* **1998**, *120*, 6024–6036.
(42) Cheng, C. F.; Zhou, W. Z.; Park, D. H.; Klinowski, J.; Hargreaves, M.; Gladden, L. F. *J. Chem. Soc., Faraday Trans.* **1997**, *93*, 359–363.

at 60 °C for 24 h in a Teflon-lined steel autoclave (Ø 1 cm, height 3 cm). After melt infiltration samples were stored under ambient atmosphere in Teflon sealed vials. The infiltrated sample was transferred to a fluidized-bed reactor and calcined by heating to 350 °C (1 °C/min, 1 h) in a flow of N_2 or 1% v/v NO/N_2 (150 mL/min for 150 mg precursor loaded catalyst). A N_2 flow was used to prevent extensive redistribution and agglomeration of Co_3O_4 during calcination, while an NO/N_2 flow was applied to achieve a high metal oxide dispersion, as has been reported by Sietsma et al.[43]

Support Characterization. N_2-Physisorption measurements were performed at −196 °C using a Micromeritics Tristar 3000. The samples were dried prior to the measurement under an N_2 flow at 250 °C for at least 12 h. The total microporous and mesoporous volume (V_p) was determined using the t-plot method at thicknesses in the range of 1.0−1.4 nm.[44] For the ordered mesoporous silica supports, the pore size distribution was calculated from the adsorption branch of the isotherm by a NL-DFT method designed for N_2 in cylindrical pores.[45] The pore size distribution of the silica gel was calculated from the desorption branch by BJH analysis. The maximum of the pore size distribution was taken as the average pore diameter.

Long range pore ordering was confirmed with low-angle X-ray diffraction. Patterns were obtained at room temperature from 0.5 to 8° 2θ with a Bruker-AXS D8 Advance X-ray Diffractometer using Co−$K_{\alpha 12}$ radiation.

Differential Scanning Calorimetry. The melting behavior of $Co(NO_3)_2 \cdot 6H_2O$ in the presence of mesoporous silica was studied with DSC (Q2000, TA Instruments). The temperature and heat flow were calibrated with a certified indium sample and measurements were performed with hermetically sealed aluminum pans (T_{zero}, ∼40 μL) under a flow of N_2 (50 mL/min). Sample masses were typically between 3−10 mg. To study the pore loading of S100 with $Co(NO_3)_2 \cdot 6H_2O$, mixtures of 0.45, 0.92, 1.4, 1.6, 1.8, and 2.7 g/g_{S100} were prepared. To determine maximum precursor loading of different supports, mixtures of $Co(NO_3)_2 \cdot 6H_2O$/support were prepared with the same salt volume/pore volume ratio as the maximum loading of S100. Melt infiltration was followed in situ for the $Co(NO_3)_2 \cdot 6H_2O$/support physical mixtures by a heat−cool-heat cycle to 75, −90, and 75 °C, respectively, at 2.5 °C/min with 5 min isothermal steps at each temperature extreme. The melting behavior of $Co(NO_3)_2 \cdot 6H_2O$ in samples that were melt infiltrated in an autoclave was followed during a single heating run to 75 °C. To detect the depressed melting point of intraporous salt, the samples were first cooled to −90 °C.

The amount of residual extraporous $Co(NO_3)_2 \cdot 6H_2O$ was calculated from the bulk melting enthalpy of $Co(NO_3)_2 \cdot 6H_2O$ in the second heating run for the in situ experiments or during the single heating run for the melt infiltrated samples. The melting enthalpy of $Co(NO_3)_2 \cdot 6H_2O$ at ∼55 °C was measured by integration using Universal Analysis 2000 (TA Instruments) with a sigmoidal baseline. The mass of extraporous $Co(NO_3)_2 \cdot 6H_2O$ was subsequently calculated with the specific melting enthalpy ($\Delta H_m = 142.9$ J/g).[46] The degree of pore-loading was expressed as the amount of intraporous $Co(NO_3)_2 \cdot 6H_2O$ ($= m_{added\ CoN} - m_{extrap\ CoN}$) in $g/g_{support}$.

Catalyst Characterization. Thermal gravimetric analysis (TGA, Q50, TA Instruments) was used to determine the weight loss of melt infiltrated samples by heating to 500 °C at 10°/min for 60 min. XRD patterns were recorded for all catalysts between 30 and 60° 2θ with a Bruker-AXS D8 Advance X-ray Diffractometer using Co−$K_{\alpha 12}$ radiation. The volume averaged Co_3O_4 crystallite size was determined for calcined catalysts using line broadening analysis on the (110), (111), and (200) peaks by a fitting procedure in Eva2 software (Bruker AXS) and the Scherrer equation with a shape factor $k = 0.9$. Long range pore ordering of the supports was confirmed with low-angle XRD. Transmission electron microscopy was performed on a Technai 20 FEG microscope operated at 200 keV as well as on a Technai 12 microscope operated at 120 keV.

Table 1. Structural Characterization of Different Mesoporous Supports and $Co(NO_3)_2 \cdot 6H_2O$ Pore-Loading ($g/g_{support}$) after Melt Infiltration at 60 °C for 24 h in an Autoclave and Corresponding Co Loading (wt%) of the Reduced Catalyst

	pore diameter	V_p[a]	maximum loading	
support	(nm)	(cm^3/g)	($g/g_{support}$)	(wt% Co)
MCM	4.5	0.87	1.2	19.5
S50	7.1	0.41	0.58	10.5
S100	11	0.96	1.4	22.1
S120	12	0.94	1.3	20.8
silica gel	12	0.80	1.1[b]	18.2

[a] Sum of microporous and mesoporous volume determined with t-plot method. [b] Calculated from melt infiltration with 100% V_{CoN}/V_p.

Catalytic Testing. Fischer−Tropsch synthesis was performed at 220 °C and 1 bar with an H_2/CO ratio of 2 v/v (3.0/1.5 mL/min). Typically, a plug-flow reactor was loaded with 15 mg of catalyst diluted with 200 mg SiC (200 μm). The catalysts were reduced in situ at 500 °C (5 °C/min, 2 h) under a flow of H_2/Ar (20/40 mL/min). Online gas chromatography analysis (C_1-C_{16}, CP sil-5, Varian) was performed during the FT reaction to determine the activity expressed as cobalt time yield (10^{-5} $mol_{CO}/g_{Co}/s$) and the C_1/C_{5+} selectivity (in wt%). The reported data were obtained after 15 h reaction time at CO conversions below 10%.

Results & Discussion

Ordered mesoporous silica supports with different pore sizes and a commercially available silica gel were used for this study of melt infiltration. A large pore MCM-41 was synthesized as well as SBA-15 at different crystallization temperatures to vary the pore diameters. The total microporous and mesoporous volume and pore diameters as characterized with N_2-physisorption are listed in the first two columns of Table 1.

The extent of pore loading of mesoporous silica with cobalt nitrate salt by melt infiltration was determined with DSC by quantifying the residual extraporous $Co(NO_3)_2 \cdot 6H_2O$ after melt infiltration. Ordered mesoporous silica S100 was mixed with increasing amounts of $Co(NO_3)_2 \cdot 6H_2O$, indicated by the mass loading in g/g_{S100}. The heat flows recorded during two subsequent heating cycles are shown in Figure 1. In the first heating cycle, a melting peak was observed at ∼53 °C for all mixtures, which corresponded to the melting of crystalline, extraporous $Co(NO_3)_2 \cdot 6H_2O$. For loadings above 1.4 g/g_{S100}, a melting peak remained at ∼53 °C in the second heating run indicating the presence of residual extraporous $Co(NO_3)_2 \cdot 6H_2O$. However, melting of $Co(NO_3)_2 \cdot 6H_2O$ at ∼53 °C vanished for loadings at 1.4 g/g_{S100} and lower, implying all salt had entered the pores. During the second heating run, melting was also observed between 5 and 20 °C which was ascribed to melting of confined or intraporous $Co(NO_3)_2 \cdot 6H_2O$.

The energy released by the melting of residual $Co(NO_3)_2 \cdot 6H_2O$ at ∼53 °C in the second heating run was used to calculate the amounts of extraporous and intraporous cobalt nitrate. In Figure 2, the amount of intraporous salt in g/g_{S100} is plotted as a function of the amount of $Co(NO_3)_2 \cdot 6H_2O$ present. In these in situ melt infiltration experiments the pore-loading reached a plateau at 1.4 g/g_{S100} which corresponds to 22 wt % Co, indicating the pores were maximally filled. Samples prepared

(43) Sietsma, J. R. A.; Meeldijk, J. D.; den Breejen, J. P.; Versluijs-Helder, M.; van Dillen, A. J.; de Jongh, P. E.; de Jong, K. P. *Angew. Chem., Int. Ed.* **2007**, *46*, 4547–4549.
(44) Lippens, B. C.; de Boer, J. H. *J. Catal.* **1965**, *4*, 319–323.
(45) Jarionec, M.; Kruk, M.; Olivier, J. P.; Koch, S. *Stud. Surf. Sci. Catal.* **2000**, *128*, 71–80.
(46) Guion, J.; Sauzade, J. D.; Laugt, M. *Thermochim. Acta* **1983**, *67*, 167–179.

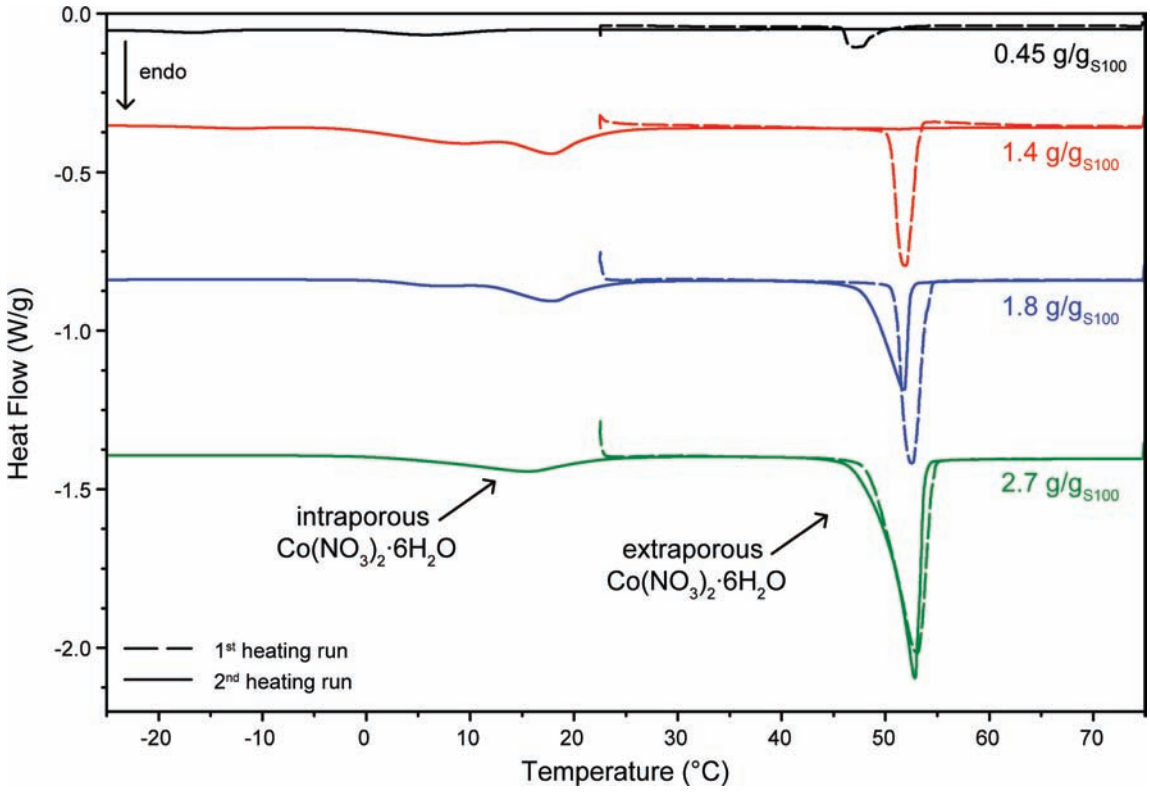

Figure 1. DSC thermograms of $Co(NO_3)_2 \cdot 6H_2O$/S100 physical mixtures with increasing amounts of $Co(NO_3)_2 \cdot 6H_2O$ (g/g_{S100}) recorded during heating at 2.5 °C/min, thermograms are offset for clarity.

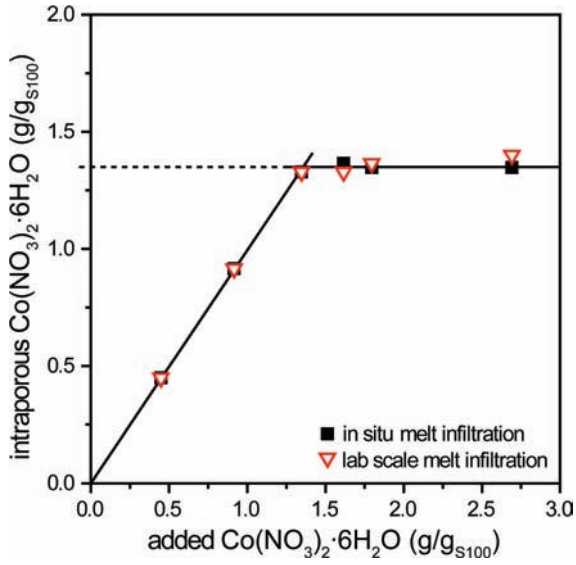

Figure 2. Amount of intraporous salt in $Co(NO_3)_2 \cdot 6H_2O$/S100 mixtures with increasing amounts of $Co(NO_3)_2 \cdot 6H_2O$ (g/g_{S100}) obtained with DSC after in situ melt infiltration and after melt infiltration in an autoclave at 60 °C for 24 h. Lines are added as guide for the eye.

ex situ by melt infiltration at 60 °C in an autoclave were also analyzed, to determine if the same maximum was obtained. The melting of surplus $Co(NO_3)_2 \cdot 6H_2O$ after the lab heat treatment was quantified during a single heating run with DSC. The pore-loading is plotted in Figure 2 and reached the same plateau at 1.4 g/g_{S100}. Furthermore, the degree of pore-filling could not be improved by additional mixing or remelting the samples. Therefore, 1.4 g/g_{S100} or 22 wt % Co was the practical loading limit for S100. If the intraporous phase was considered to be crystalline $Co(NO_3)_2 \cdot 6H_2O$ with a density of 1.88 g/cm^3, then this would correspond to a filling of 75% of the pore volume.

The quantification of pore-filling was based on the melting enthalpy of residual extraporous $Co(NO_3)_2 \cdot 6H_2O$. However, wetting of the external surface of the mesoporous silica by extraporous $Co(NO_3)_2 \cdot 6H_2O$ caused broadening and a slight shift to lower temperatures of the melting peak at ~53 °C. Nevertheless, since the mesoporous silica supports have low external surface areas, the effect on the calculated degree of pore-filling was expected to be within the error of the measurements and therefore neglected. Furthermore, the energy released in the first heating run was much lower than the enthalpy expected from melting of all present $Co(NO_3)_2 \cdot 6H_2O$. This was also observed for other infiltration experiments[47] and indicated that wetting and infiltration into the pores is an exothermic process occurring simultaneously with the endothermic melting of extraporous $Co(NO_3)_2 \cdot 6H_2O$.

To study the effect of pore size on melt infiltration and the extent of pore-filling, mesoporous silica supports with different pore radii and pore geometries were infiltrated with $Co(NO_3)_2 \cdot 6H_2O$ at 60 °C for 24 h in an autoclave. The maximum loading of S100 corresponded to a theoretical pore volume filling of 75%, if the intraporous phase was considered to be crystalline $Co(NO_3)_2 \cdot 6H_2O$. Therefore, an intended loading of 75% V_{CoN}/V_p was used for the other supports. After melt infiltration, the pore-filling was studied with DSC during a single heating run from −90 to 75 °C and Figure 3 shows the recorded thermograms. The maximum precursor loading for the different supports was calculated in $g/g_{support}$ and is listed in Table 1,

(47) Adelhelm, P.; Gao, J. B.; Verkuijlen, M. H. W.; Rongeat, C.; Herrich, M.; van Bentum, P. J. M.; Gutfleisch, O.; Kentgens, A. P. M.; de Jong, K. P.; de Jongh, P. E. *Chem. Mater.* **2010**, *22*, 2233–2238.

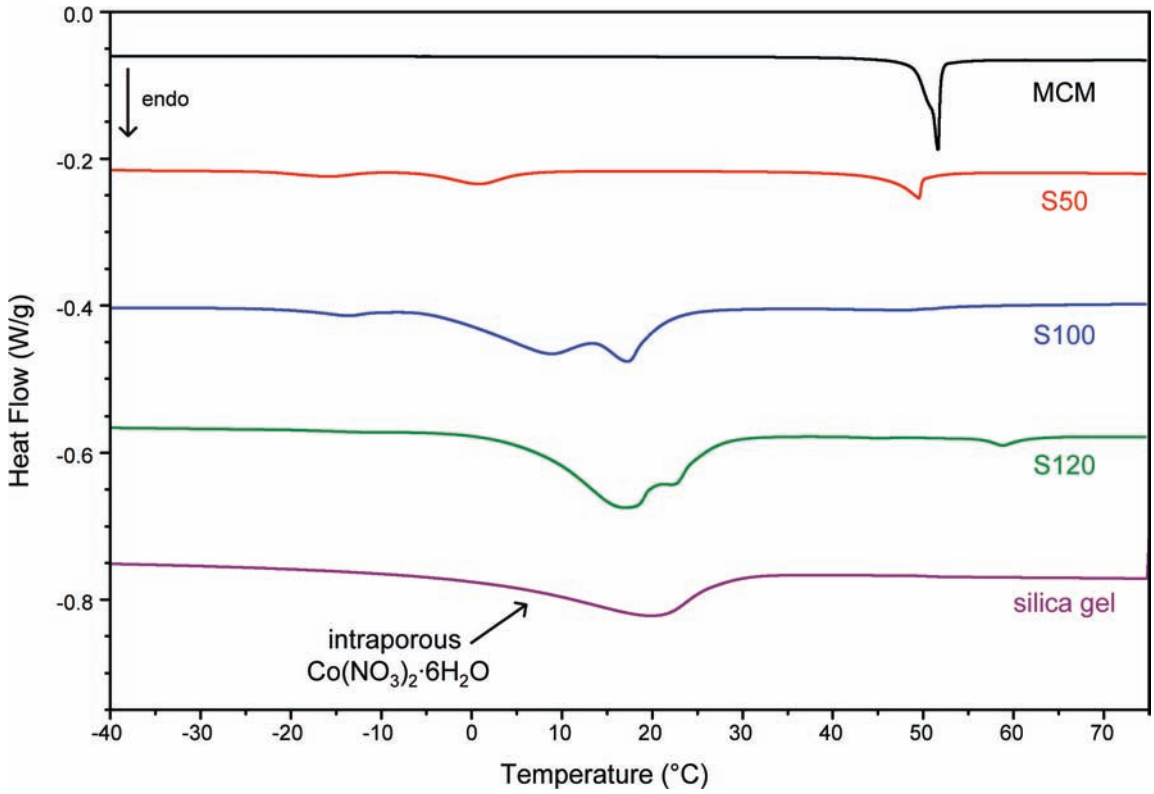

Figure 3. DSC thermograms of different silica supports melt infiltrated with $Co(NO_3)_2 \cdot 6H_2O$ (amount corresponding to practical filling limit S100) in an autoclave at 60 °C for 24 h, recorded during heating at 2.5 °C/min, thermograms are offset for clarity.

together with the corresponding cobalt weight loadings. If the intraporous phase is considered to be crystalline $Co(NO_3)_2 \cdot 6H_2O$, then the pore-filling ranged from 70% to 80% of the microporous and mesoporous volume and was slightly dependent on the pore diameters. For MCM, a melting peak remained at ~53 °C corresponding to a filling lower than 75%. Since the specific melting enthalpy of extraporous $Co(NO_3)_2 \cdot 6H_2O$ is at least an order of magnitude larger than for intraporous $Co(NO_3)_2 \cdot 6H_2O$, the bulk melting peak appeared to be relatively large compared to other pore melting peaks. Nevertheless, the melting peak at ~53 °C corresponds to only 7 wt % of the total amount of $Co(NO_3)_2 \cdot 6H_2O$ added. For all samples, the weight loss determined with TGA confirmed the composition of $Co(NO_3)_2 \cdot 6H_2O$. In a control experiment, all $Co(NO_3)_2 \cdot 6H_2O$ was dissolved after melt infiltration of MCM. The pore volume of MCM was recovered within 5% of the parent pore volume, indicating that the physical mixing and melt infiltration did not significantly damage the pore structure.

The melting transitions corresponding to intraporous $Co(NO_3)_2 \cdot 6H_2O$ were very broad and consisted of multiple peaks for some supports, indicating that inside the pores a single crystalline phase had not formed. They shifted to lower temperatures as the pore diameter decreased. Also, the melting enthalpy for intraporous $Co(NO_3)_2 \cdot 6H_2O$ decreased with decreasing pore diameter due to an increasing ratio of $Co(NO_3)_2 \cdot 6H_2O$ interacting with the silica pore wall to the crystallizing intraporous $Co(NO_3)_2 \cdot 6H_2O$ phase.[48] A discrete melting transition is no longer observed for the MCM support since the pore diameter is only 3× the $Co(NO_3)_2 \cdot 6H_2O$ crystal unit cell. These effects are known for confined fluids such as water or organic solvents.[49,50] On the basis of the observations from melting of the intraporous salt, it can be concluded that the intraporous phase does not have a well-defined crystal structure and most likely does not have the density of crystalline $Co(NO_3)_2 \cdot 6H_2O$. Therefore, we propose that the extent of pore filling is actually close to 100% with a lower density disordered intraporous phase interacting with the silica surface.

The melting point of $Co(NO_3)_2 \cdot 6H_2O$ is close to its decomposition point, i.e., 55 and 74 °C, respectively. Hence, decomposition could inhibit the melt infiltration process. To ensure ample time for the liquid phase to flow into the porous system, an equilibration step at 60 °C was introduced and the effect of sample containment was studied with XRD and TEM. Figure 4 shows the XRD patterns recorded after 12 h at 60 °C in an open crucible and in a closed autoclave. During open melt infiltration, $Co(NO_3)_2 \cdot 6H_2O$ had dehydrated to $Co(NO_3)_2 \cdot 4H_2O$. The sharp diffraction lines indicated that this phase was not confined within the pore system. After melt infiltration in the closed autoclave no crystalline phases were observed, but with TGA the presence of $Co(NO_3)_2 \cdot 6H_2O$ and a small amount of physisorbed water on the silica was confirmed.

XRD at low scattering angles was used to obtain complementary information to DSC on the pore-filling after open and closed melt infiltration. As shown in Figure 5, no diffraction lines were recorded after melt infiltration in an autoclave, but were present after open melt infiltration. Nevertheless, the long-range ordering of the parent S100 was apparent in the physical mixture (data not shown) as well as after closed melt infiltration

(48) Morishige, K.; Nobuoka, K. *J. Chem. Phys.* **1997**, *107*, 6965–6969.
(49) Kittaka, S.; Ishimaru, S.; Kuranishi, M.; Matsuda, T.; Yamaguchi, T. *Phys. Chem. Chem. Phys.* **2006**, *8*, 3223–3231.
(50) Jahnert, S.; Chavez, F. V.; Schaumann, G. E.; Schreiber, A.; Schonhoff, M.; Findenegg, G. H. *Phys. Chem. Chem. Phys.* **2008**, *10*, 6039–6051.

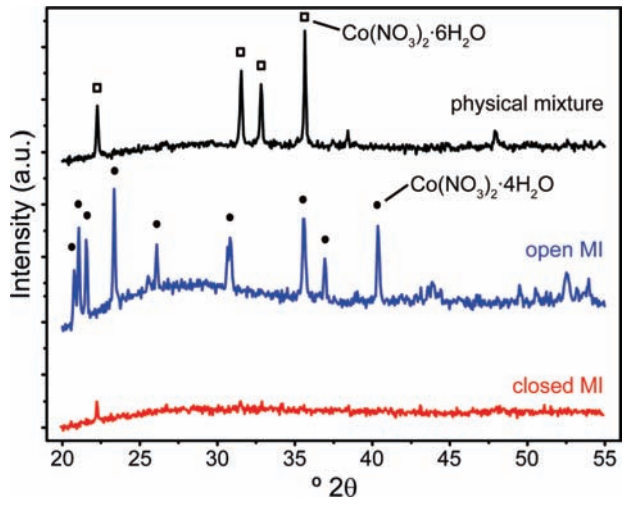

Figure 4. XRD patterns of $Co(NO_3)_2 \cdot 6H_2O$/S100 (1.4 g/g_{S100}) physical mixture and after open melt infiltration in a crucible and closed melt infiltration in an autoclave at 60 °C for 12 h.

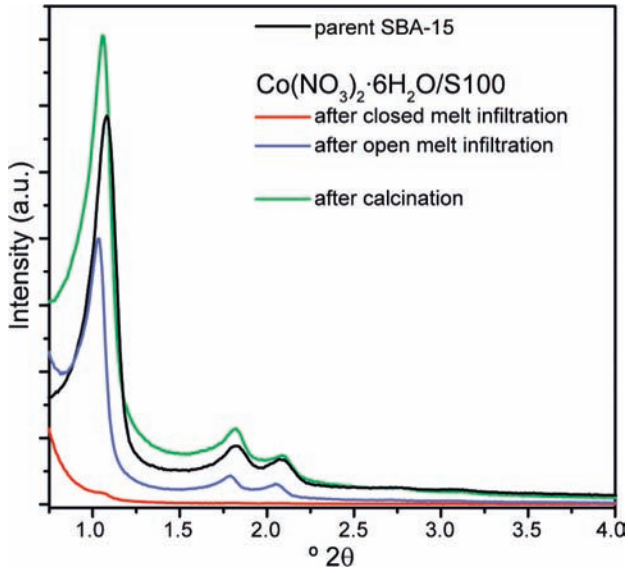

Figure 5. Low angle XRD patterns for $Co(NO_3)_2 \cdot 6H_2O$/S100 (1.4 g/g_{S100}) after open melt infiltration in a crucible and closed melt infiltration in an autoclave at 60 °C for 12 h and Co_3O_4/S100 prepared via closed melt infiltration and calcination in N_2 flow.

and calcination in N_2 flow. Therefore, the hexagonal pore ordering of the SBA-15 support was not destroyed by the melt infiltration procedure. Rather, the loss of diffraction lines after closed melt infiltration was caused by filling of the pores with $Co(NO_3)_2 \cdot 6H_2O$. The diffraction lines for ordered mesoporous silica originate from the difference in electron density of the silica matrix and the contents of the pores, i.e., air in case of the parent material and the calcined sample. When the pores are filled with a material of comparable electron density to the silica matrix, e.g., amorphous $Co(NO_3)_2 \cdot 6H_2O$, the contrast diminishes and diffraction of the ordered pore system can no longer be observed. For that reason, it can be concluded that the pores of S100 after melt infiltration with $Co(NO_3)_2 \cdot 6H_2O$ in a closed vessel are filled, such that there is no long-range ordering of empty pores. The clear diffraction pattern after open melt infiltration indicated that a fraction of the pores remained empty. This is in line with the formation of extraporous tetra hydrate cobalt nitrate observed in XRD at higher angles.

The distribution of Co_3O_4 over the support particles after calcination in a N_2 flow was visualized with TEM and could be correlated to the precursor distribution after open and closed melt infiltration. Figure 6A shows a typical image for Co_3O_4/S100 infiltrated with cobalt nitrate in an autoclave. It shows aggregates of pluglike Co_3O_4 particles present in several neighboring pores (vide infra). These aggregates were observed throughout the support particle. Even though the distribution of Co_3O_4 over the support particle was inhomogeneous, it was all intraporous after calcination and all the support particles contained similar loadings. Therefore, the precursor had been present as intraporous phase in all the support particles prior to calcination. Figure 6B,C shows two micrographs of Co_3O_4/S100 prepared via open melt infiltration. In Figure 6B, a support particle is shown with intraporous aggregates similar to Figure 6A. However, also some extraporous aggregates were observed, which are indicated by the arrows in Figure 6B,C. In addition, Figure 6C shows some empty support particles, which illustrate the large variation of Co_3O_4 loading over the support particles in the sample. It suggested that the precursor had not infiltrated all of the support particles and that open melt infiltration led to an inhomogeneous precursor distribution over the support. Therefore, to obtain a homogeneous distribution of the metal oxide over the support after calcination, decomposition of the precursor during melt infiltration should be prevented. Please note that although NO/N_2 calcination leads to high metal oxide dispersions (vide infra) it does not bring about redistribution of previously nonuniform cobalt nitrate distributions.

To prepare Co/SiO_2 catalysts for the Fischer−Tropsch synthesis, different supports were melt infiltrated with $Co(NO_3)_2 \cdot 6H_2O$ at 60 °C for 24 h in an autoclave. After calcination in a N_2 flow, the Co_3O_4 loaded catalysts were characterized with XRD and TEM. The metal loadings ranged from 10−22 wt % depending on the support pore volume. The volume-average Co_3O_4 crystallite sizes, calculated with the Scherrer equation, were taken as a measure for the dispersion and are listed in Table 2. Their sizes ranged from 4−10 nm and generally followed the support pore diameters or were slightly smaller than the pore diameter for the larger pore systems. This showed that the average crystallite sizes could be well controlled through the mesoporous supports as was also reported for impregnated systems.[40] Also on the industrial silica gel support, highly dispersed Co_3O_4 was obtained, even though this support has a much broader pore size distribution than the ordered supports. Additional control over the Co_3O_4 crystallite size was obtained by using the modified calcination procedure in 1% NO/N_2,[40,43] which resulted in a decrease of the average crystallite size from 9.5 to 4.3 nm on S100.

The Co_3O_4 nanoparticle distribution over the support was visualized with TEM. The high metal loadings hindered accurate particle size analysis with TEM, however, Co_3O_4 crystallites were typically observed confined within the pore system with sizes in the same range as the pore diameter. Figure 7 shows typical micrographs for Co_3O_4/S100 obtained via melt infiltration in an autoclave after calcination in N_2 (Figure 7A) or in 1% NO/N_2 (Figure 7B). N_2-calcination led to the formation of pluglike nanoparticles inside the pore system, which formed aggregates that spanned multiple pores. The formation of these pluglike nanoparticles after calcination in N_2 was visualized earlier with electron tomography for NiO on SBA-15[51] and similar intraporous aggregates have often been observed for Co/SiO_2 systems prepared via impregnation and calcination.[52−54]

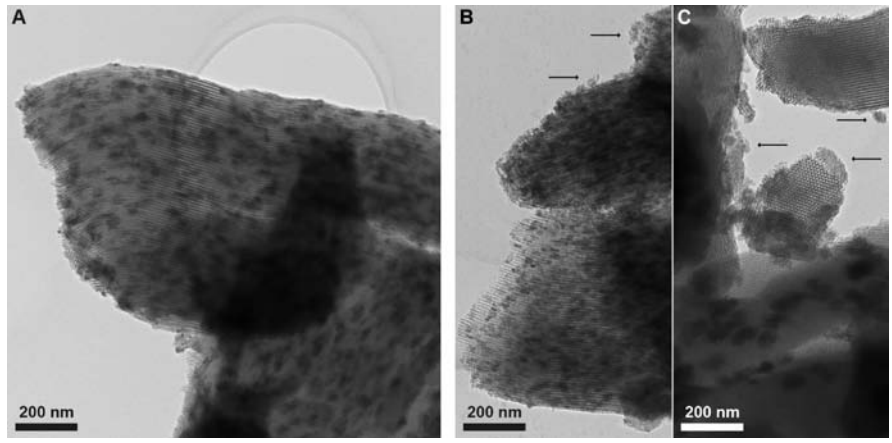

Figure 6. TEM micrographs of Co_3O_4/S100 after calcination in N_2 prepared via closed melt infiltration (A) and prepared via open melt infiltration (B and C). Arrows indicate extraporous Co_3O_4.

Table 2. Characterization and Catalytic Activity for Fischer−tropsch Synthesis of Catalysts Prepared via Melt Infiltration in an Autoclave at 60 °C for 24 H and Calcination in N_2

	Co loading	pore diameter	Co_3O_4	CTY[b]	selectivity
support	(wt%)	(nm)	crystallite size[a] (nm)	(10^{-5} $mol_{CO}/g_{Co}/s$)	C_1/C_{5+} (wt%)
MCM	19.9	4.5	4.9	1.0	35/39
S50	10.5	7.1	7.8	1.8	29/44
S100	21.7	11	9.5	1.3	27/45
S120	21.2	12	8.3	2.7	28/43
silica gel	17.6	12	8.0	2.1	22/54
S100[c]	21.7	11	4.3	3.0	34/36

[a] Determined with XRD line broadening analysis after calcination in N_2 flow. [b] Catalytic properties determined after 15 h time on stream. [c] Calcined in 1% v/v NO/N_2 flow.

Calcination in 1% NO/N_2 led to the formation of individual Co_3O_4 nanoparticles, which has also been observed for NiO/SBA-15 and Co_3O_4/SBA-15 prepared via impregnation.[40,43] This confirms that after melt infiltration the Co_3O_4 dispersion and distribution is affected strongly by the calcination conditions as well as confinement. The possibility to tune the nanoparticle size and distribution after melt infiltration is essential for its application in supported catalyst preparation.

The activity of the catalysts for the Fischer−Tropsch synthesis was tested after in situ reduction at 500 at 220 °C and 1 bar. The obtained cobalt weight normalized activities (CTY) and selectivity are listed in Table 2. For the N_2-calcined samples, moderate (MCM, S50) to high activities (S120) were observed, as compared to the most active Co/CNF catalyst (CTY reported 3.5×10^{-5} $mol_{CO}/g_{Co}/s$).[55,56] For the Co/S100 N_2-calcined catalyst a dispersion of 7.2% was measured with chemisorption. This corresponds to a TOF of 11 $*10^{-3}$ s^{-1}, which is the value found for Co/CNF catalysts with particle sizes larger than 6 nm.[55,56] On the basis of the different pore diameters, pore geometries and Co_3O_4 average crystallite sizes, differences in the observed CTY are expected. Previous XANES analysis of a Co/SiO_2 catalyst with 5 nm Co particles has shown that a reduction degree of 90% is obtained after reduction at 450 °C and 2 h reaction time.[57] The catalysts presented in this work were reduced at 500 °C and had degrees of reduction close to 100%. Nevertheless, the catalytic activity can be optimized by changing for example the calcination conditions, which was shown recently by den Breejen et al.[57] Indeed, the Co/S100 NO calcined catalyst showed a much higher activity than its N_2 calcined counterpart, due to less agglomeration, a higher dispersion and a narrow particle size distribution. With TEM sintering or redistribution of the active phase upon reduction and Fischer−Tropsch synthesis were excluded (Figure S1, Supporting Information). All catalysts showed a high methane selectivity, with the lowest value observed for the industrial silica support. The selectivity is mainly related to the low pressure applied, while also pore geometry can play a role.

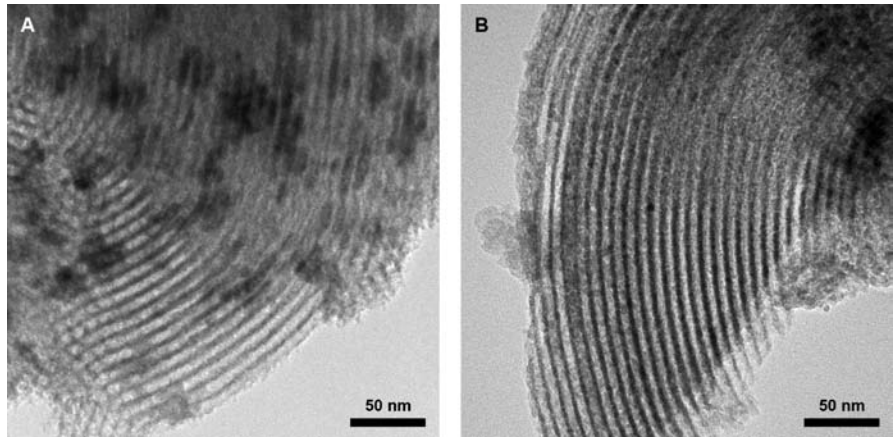

Figure 7. TEM micrographs of Co_3O_4/S100 prepared via closed melt infiltration and calcination in N_2 (A) or 1% v/v NO/N_2 (B).

Optimization of support morphology or addition of promoters could be used to improve the selectivity.[53,57]

Conclusions

We have studied in depth the physicochemical aspects of melt infiltration for preparation of supported catalysts. To establish the effectiveness of melt infiltration as a precursor loading method, infiltration of mesoporous silica supports with $Co(NO_3)_2 \cdot 6H_2O$ was followed in situ with differential scanning calorimetry. The melting point depression of intraporous $Co(NO_3)_2 \cdot 6H_2O$ allowed detection of residual extraporous $Co(NO_3)_2 \cdot 6H_2O$. Maximum precursor loadings were expressed in $g/g_{support}$ and corresponded to 70 − 80% of the pore volume, if the intraporous phase was considered to be crystalline $Co(NO_3)_2 \cdot 6H_2O$. Nevertheless, after melt infiltration at 60 °C in a closed vessel, no crystalline phases could be detected with XRD diffraction. In addition, the diffraction lines from the ordered mesoporous support at low scattering angles had disappeared. This led to the conclusion that the pores of the support were actually completely filled with an amorphous $Co(NO_3)_2 \cdot 6H_2O$ phase with a lower density than crystalline $Co(NO_3)_2 \cdot 6H_2O$. When the $Co(NO_3)_2 \cdot 6H_2O$ precursor decomposed by dehydration to $Co(NO_3)_2 \cdot 4H_2O$ during the infiltration process, melt infiltration was partly inhibited and an inhomogeneous distribution of the precursor over the support resulted.

Finally, melt infiltration was applied to prepare a series of Fischer−Tropsch catalysts with controllable particle sizes and high metal loadings. By using supports with different pore diameters, Co_3O_4 crystallite sizes ranging from 4 to 10 nm at Co loadings ranging from 10−22 wt % were obtained. After calcination in a N_2 flow, pluglike nanoparticles were obtained, while calcination in a gas flow of 1% NO/N_2 led to the formation of highly dispersed individual Co_3O_4 nanoparticles. The catalysts showed high activity for the Fischer−Tropsch synthesis, with the highest activity observed for the catalyst calcined in NO/N_2.

Acknowledgment. The authors acknowledge J. Meeldijk for performing TEM measurements and M. van Steenbergen and H. Talsma for providing access to thermal analyses equipment and useful discussions. The Netherlands Organisation for Scientific Research is thanked for funding (NWO TOP/ECHO 700.57.341).

Supporting Information Available: Figure S1, TEM micrographs of Co/S100 calcined in NO/N_2 after reduction at 500 ºC for 2 h and after Fischer−Tropsch synthesis for 20 h. This material is available free of charge via the Internet at http://pubs.acs.org.

JA1080508

(51) Sietsma, J. R. A.; Friedrich, H.; Broersma, A.; Versluijs-Helder, M.; van Dillen, A. J.; de Jongh, P. E.; de Jong, K. P. *J. Catal.* **2008**, *260*, 227–235.
(52) van der Meer, J.; Bardez, I.; Bart, F.; Albouy, P. A.; Wallez, G.; Davidson, A. *Micropor. Mesopor. Mater.* **2009**, *118*, 183–188.
(53) Prieto, G.; Martinez, A.; Murciano, R.; Arribas, M. A. *Appl. Catal. A-Gen.* **2009**, *367*, 146–156.
(54) Jiao, F.; Frei, H. *Angew. Chem., Int. Ed.* **2009**, *48*, 1841–1844.
(55) Bezemer, G. L.; Bitter, J. H.; Kuipers, H. P. C. E.; Oosterbeek, H.; Holewijn, J. E.; Xu, X. D.; Kapteijn, F.; van Dillen, A. J.; de Jong, K. P. *J. Am. Chem. Soc.* **2006**, *128*, 3956–3964.
(56) den Breejen, J. P.; Radstake, P. B.; Bezemer, G. L.; Bitter, J. H.; Froseth, V.; Holmen, A.; de Jong, K. P. *J. Am. Chem. Soc.* **2009**, *131*, 7197–7203.
(57) Den Breejen, J. P.; Sietsma, J. R. A.; Friedrich, H.; Bitter, J. H.; De Jong, K. P. *J. Catal.* **2010**, *270*, 146–152.